

Article

Electrical and Mechanical Characteristics of a High-Speed Motor for Electric Turbochargers in Relation to Eccentricity

Tae-Woo Lee ^{1,2}  and Do-Kwan Hong ^{1,2,*} 

¹ Department of Energy and Power Conversion Engineering, University of Science and Technology, Changwon 51543, Korea; twlee@keri.re.kr

² Electric Machine and Drives Research Center, Korea Electrotechnology Research Institute, Changwon 51543, Korea

* Correspondence: dkhong@keri.re.kr; Tel.: +82-(0)10-9601-9234

Abstract: As the demand for eco-friendly, high-efficiency transportation technologies increase due to climate change, a high-speed electric motor, a key component of an electric turbocharger, has been developed that can reduce emissions and increase fuel efficiency. Korea Electrotechnology Research Institute with Keyyang Precision Co., Ltd., developed a high-speed surface-mounted permanent magnet synchronous motor. It operates at a power of 3 kW at 100,000 rpm and is intended to fit 1600 cc diesel vehicles. In this paper, the electrical and mechanical characteristics of the high-speed motor were reviewed in consideration of the effect of eccentricity among the various causes that affect vibration. It was confirmed that eccentricity affected the distribution of the electromagnetic force and inductance of the winding due to the uneven air-gap. Additional vibration was generated at the half of pole passing frequency (1666.67 Hz). Diagnosing the presence or absence of eccentricity when driving a motor takes a great deal of time and cost because the load is separated or the motor is diagnosed through disassembly and measurement. The characteristics of eccentricity identified in this paper can be checked using a relatively simple method when diagnosing the presence or absence of actual eccentricity.

Keywords: eccentricity; electric turbocharger; high-speed motor; one-way coupled analysis



Citation: Lee, T.-W.; Hong, D.-K. Electrical and Mechanical Characteristics of a High-Speed Motor for Electric Turbochargers in Relation to Eccentricity. *Energies* **2021**, *14*, 3340. <https://doi.org/10.3390/en14113340>

Academic Editor: Adolfo Dannier

Received: 30 April 2021

Accepted: 1 June 2021

Published: 7 June 2021

Publisher's Note: MDPI stays neutral with regard to jurisdictional claims in published maps and institutional affiliations.



Copyright: © 2021 by the authors. Licensee MDPI, Basel, Switzerland. This article is an open access article distributed under the terms and conditions of the Creative Commons Attribution (CC BY) license (<https://creativecommons.org/licenses/by/4.0/>).

1. Introduction

The recent demand for eco-friendly, high-efficiency transportation technologies, along with the related regulations imposed on the automotive industry due to climate change, is driving research for reduction in carbon dioxide (CO₂) and for greater fuel efficiency of automobiles. The most representative way to realize these is to downsize the engine. Engine downsizing is a methodology for reducing the engine displacement to prevent fuel wasting. To compensate for the resulting insufficient performance, a great deal of fresh air is forced through the engine using turbochargers or superchargers in what are known as forced induction systems (FIS) [1]. The effect is similar to that from an increase in the exhaust capacity. A turbocharger, which reuses the exhaust gas to drive the turbine, was introduced circa 110 years ago by the Swiss engineer Alfred Büchi [2]. However, it was difficult to use in normal passenger cars because it must be accompanied by extreme heat control technology and high engine durability. In addition, the turbo lag that occurs at low speed (unlike with naturally aspirated engines) was another reason that the turbocharger was difficult to use. However, turbochargers became widely used after improvement of the engine durability and development of turbocharging technologies, including the variable geometry turbocharger (VGT), 2-stage turbocharger (twin turbocharger), and electric turbocharger (ETC), which could reduce turbo lag. Ultimately, these technologies are expected to evolve into an electric turbocharger technology. This is because the electric motor is capable of producing maximum torque from the moment current is applied. This can effectively reduce turbo lag by rapidly rotating the turbine even at a low engine speed

with low exhaust gas. This electric motor is not always running: it is designed to run only early in the initial acceleration stage to eliminate the turbo lag. The literature and research on electric turbochargers for vehicles with 12 V to 48 V battery systems from the last 20 years are shown in Figure 1 and Table 1 [1,3–22].

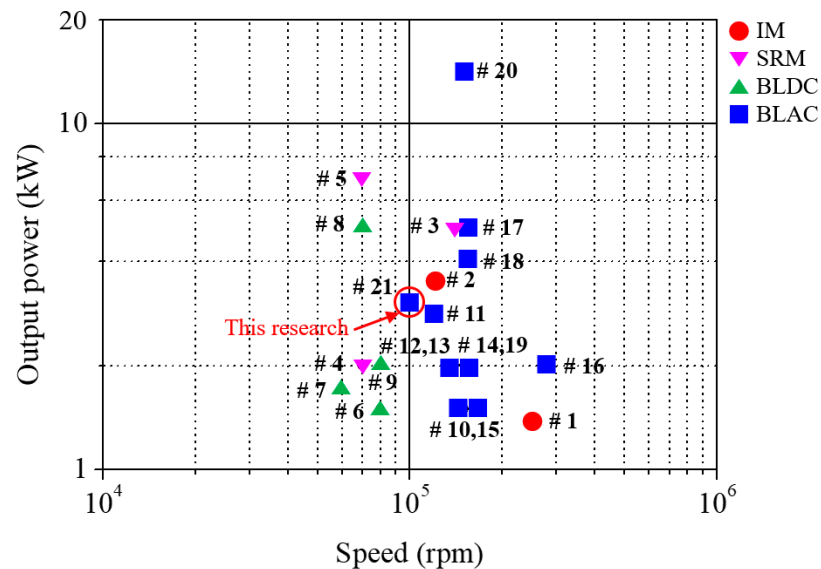


Figure 1. High-speed motors of electric turbocharger output power versus speed for different machine topologies.

Table 1. High-speed machines for electric turbochargers with 12 V to 48 V battery systems.

No.	Motor	Power [kW]	Speed [krpm]	Voltage [Vdc]	Topology	Designed/Studied by
1	IM	1.4	250	12	EAT	Honeywell
2		2.8	120	48	EAT	Honeywell
3 ¹	SRM	5.0	140	12/24	EAT	Loughborough Univ.
4		2.0	70	12	TEDC	Valeo/CPT
5 ²		7.0	70	48	TEDC	Valeo/CPT
6	BLDC	1.5	80	24	TEDC	WEM-PEC
7		1.7	60	12	TEDC	BorgWarner
8 ³		5.0	70	48	TEDC	BorgWarner
9		2.0	80	48	TEDC	MMT
10	BLAC	1.5	150	12	EC	Nagaoka Univ.
11		3.5	120	48	EC	Technische Univ.
12		2.0	140	12	EC	MHI
13		2.0	140	12	EAT	MHI
14		2.0	150	12	EAT	IHI
15		1.5	160	12	EAT	G+L innotec
16		2.0	280	12	EAT	EcoMotor
17		5.0	150	48	EAT	EcoMotor
18		4.0	150	48	EAT	Hanyang Univ.
19		2.0	150	12	EAT	Aeristech
20		14.0	150	48	EAT	Aeristech
21	3.0	100	48	TEDC	KERI/Keyyang	

¹ Applied to Caterpillar 7.01 L heavy duty vehicles diesel engine. ² Applied to Audi SQ7 4.0 L TDI engine.

³ Applied to Mercedes-Benz 3.0 L M256 engine.

In Table 1, the high-speed motors used in electric turbochargers are categorized as induction motors (IM), switched reluctance motors (SRM), and permanent magnet synchronous motors (PMSM). The IMs are suitable for the high mechanical stress that accompanies high-speed operation because they are durable and structurally robust. Because the rotor does not use PMs, it is a good candidate for electric turbochargers that are exposed to high-temperature environments. However, their efficiency is relatively low due

to additional losses from rotor current. SRMs are also suitable for electric turbochargers used in high-speed operation and at high ambient temperature because of the absence of PMs in the rotor. However, due to the torque generation principle, the stator inductance changes very non-linearly according to the magnitude of the excitation current and the relative position of the rotor and stator. Thus, the torque generated is proportional to the time variation of the inductance, resulting in non-uniform rotational force. This causes torque ripple, resulting in severe noise and vibration, and reduces efficiency. PMSMs, including brushless AC and DC (BLAC and BLDC) motors, have a high power density and efficiency because they use rare earth magnets with high energy integration. With these advantages, miniaturization and weight reduction are possible. However, there is also a disadvantage in that the price is increased because the rare earth magnet is used. In the case of an electric turbocharger used in a high-temperature environment, in particular, PMs with a high working temperature must be used to prevent demagnetization. In the case of surface mounted permanent magnet synchronous motors (SPMSM), a retainer (or sleeve) is required to prevent the PMs from scattering [22]. W. Lee et al. well described the topology of electric forced induction systems (EFIS) according to the location of the electric motor: electric compressor (EC), electrically assisted turbocharger (EAT), electrically split turbocharger (EST), and turbocharger with an additional electrically driven compressor (TEDC) [1]. Therefore, it is necessary to select an appropriate type of motor and EFIS topology by carefully considering their advantages and disadvantages.

This study was conducted by those at the Korea Electrotechnology Research Institute (KERI) along with those at the Keyyang Precision Co., Ltd. (manufacturer of conventional turbochargers in Gimcheon-si, Gyeongsangbuk-do, South Korea). Together, they developed a high-speed surface mounted permanent magnet synchronous motor (SPMSM) and a pulse width modulation (PWM) driven inverter. These provided high power density and efficiency to drive a turbocharger with an additional electrically driven compressor (TEDC) added upstream. In Table 1, the topology of most electric turbochargers is EAT or TEDC. The reasons for choosing TEDC rather than EAT are as follows. First, with TEDC it is easy to assure thermal stability because the electric motor is separate from the conventional turbocharger. Second, it has the advantage of improving transient response because the electric motor is separate. On the other hand, in the case of using PMs in the EAT topology, it is not easy to secure thermal stability because the motor is located on the conventional turbocharger shaft. That is, the moment of inertia of the shaft increases, which is disadvantageous in terms of transient response. Our electric turbocharger system operates at a power of 3 kW at 100,000 rpm and is intended to fit 1600 cc diesel vehicles to reduce turbo lag to within 0.4 s, as shown in Figure 2 [17,21,22].

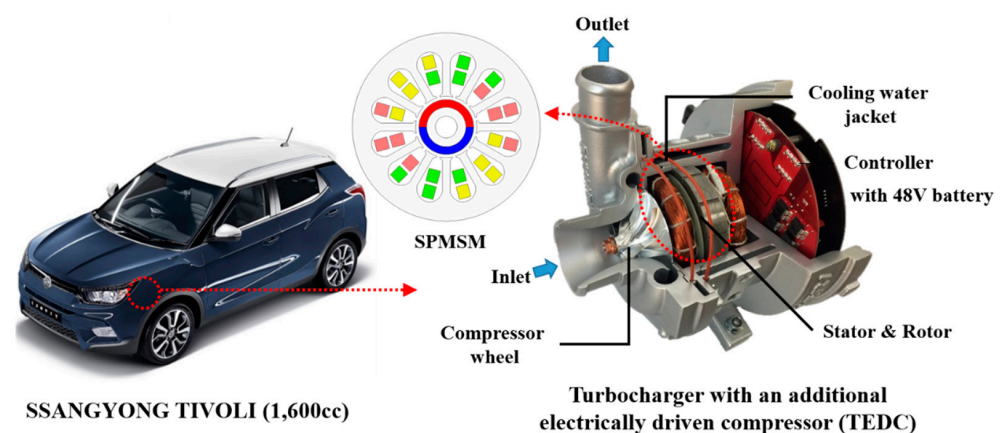


Figure 2. KERI and Keyyang Precision’s turbocharger with an additional electrically driven compressor (TEDC).

When designing a high-speed PM motor, it is important to select an appropriate material considering the operating environment and conditions, and other characteristics

according to the pole–slot combination. In addition, it is necessary to consider a structure that can withstand the centrifugal force generated by high-speed operation and that is robust against vibration and noise. Selection of bearings suitable for these operating conditions is also important. In this paper, the pole–slot combination and winding topology were selected after considering the pertinent electromagnetic characteristics. Then, the electrical characteristics according to eccentricity were analyzed using ANSYS Maxwell, and the mechanical characteristics were also analyzed using an ANSYS mechanical module by mapping non-uniform electromagnetic force (one-way coupled) due to eccentricity of the 3-dimensional (3D) model.

2. Selection of the Pole–Slot Combination and Winding Topology

One of the ways to maximize the power density is to increase the number of poles of a PM motor. If there is a motor with the same saturation magnetic flux density at the tooth and stator yoke, a design for one that increases the number of poles decreases the outer diameter of the stator. If the magnetic and electric loadings are increased, the size of the motor decreases and the power density can be improved. However, when considering the controllability of the motor, increase in the number of poles is limited. If the number of switching possible for control of the sinusoidal current is 10 to 20 times per period, the number of poles is dependent on the maximum operating speed. Considering the above conditions, the number of poles that can be used in a high-speed motor is between 2 and 4 poles [23]. Because the motor characteristics vary depending on the pole–slot combination, it is important to determine the optimal number of slots. The number of slots should be determined with consideration of factors such as cogging torque, winding configuration, winding factor, the number of turns, power density, radial force, mechanical structure, and manufacturing cost. The latter should be based on whether a given winding can be produced using automation or if manual labor is required [24].

Before determining the optimal number of slots, it is first necessary to determine which winding methods to use, such as concentrated winding or distributed winding. Distributed winding, known as overlapping winding, is made with the winding pitch equal or slightly shorter than the pole pitch. Such windings have a relatively high winding factor. A disadvantage of this winding configuration is the long end coil, which causes copper loss and consumption. On the other hand, the concentrated windings, referred to as tooth-coil or non-overlapping windings, are usually made by putting conductors around a single stator tooth [24]. Compared to the distribution windings, the concentrated windings have a higher slot fill factor and less end coil, smaller copper loss, and excellent fabrication. However, they require a higher number of turns (or increase in the stack length) to generate the same torque as an equivalent motor with overlapping windings due to their relatively low winding factor. Moreover, they have large harmonic components [24].

In the work reported in this paper, the number of poles was fixed to 2. The number of slots was changed from 3 to 12 with a multiple of three, and both concentrated and distributed windings were applied by adjusting the coil span. Among the possible combinations, when the pole pitch (number of slots/number of poles) was fractional, only the concentrated winding was applied. When the pole pitch was an integer, both concentrated and distributed windings were applied. Among these options, only those with a winding factor (calculated using Equation (1)) of 0.866 or more, are shown in Table 2.

$$k_{wh} = k_{ph}k_{dh}, k_{ph} = \cos\left(h\frac{\gamma}{2}\right), k_{dh} = \frac{\sin\left(\frac{hq\gamma}{2}\right)}{q\sin\left(\frac{h\gamma}{2}\right)}, q = \frac{N_s}{3P} \quad (1)$$

where k_{wh} is the winding factor while k_{ph} and k_{dh} are the pitch factor and distribution factor, respectively. The term h is the harmonics order, q is the slot per phase per pole, γ is the slot pitch, N_s is the number of slots, and P is the number of poles [25].

$$\begin{aligned}
 MMF_a &= \frac{4}{\pi} \frac{N i_a}{2} \sum_h \frac{1}{h} k_{ph} k_{dh} \cos[h\omega t] \\
 MMF_b &= \frac{4}{\pi} \frac{N i_b}{2} \sum_h \frac{1}{h} k_{ph} k_{dh} \cos[h\omega t - \frac{2\pi}{3}] \\
 MMF_c &= \frac{4}{\pi} \frac{N i_c}{2} \sum_h \frac{1}{h} k_{ph} k_{dh} \cos[h\omega t + \frac{2\pi}{3}]
 \end{aligned} \tag{2}$$

Table 2. Pole–slot combinations according to winding topology.

No.	Poles	Slots	Coil Span	Topology	Winding Factor
1	2	3	1	Concentrated	0.866
2	2	6	2	Distributed (short)	0.866
3	2	6	3	Distributed (full)	1
4	2	12	5	Distributed (short)	0.933
5	2	12	6	Distributed (full)	0.966

The stator winding magnetomotive force (MMF) in a three-phase motor is calculated using (2), where N is the number of turns and ω is the excitation angular velocity [26]. In studies of the spatial harmonic distribution, the harmonic component at the lowest order is defined as the fundamental component. It has an order of $h = P/2$. To illustrate the difference between the five cases considered, Figure 3 and Table 3 show relative amplitudes (with respect to the fundamental) under 15th harmonics in the winding spatial distribution. Spatial harmonics that are multiples of three are not listed in the table because they do not create a net stator field [24,25]. Four cases (except Case 1) contain $6h \pm 1$ st order harmonics (Table 3). The losses in Case 1 are expected to be greater than in other cases because it contains $6h \pm 1$ st order harmonics, as well as additional even-order harmonics. To compare the electromagnetic performance of these five cases, the inner, outer diameters, and the stack length of the stator were kept the same, and the number of turns in series was also the same. The tooth width was adjusted according to change in the number of slots, and the thickness of the back yoke was kept constant. To obtain the same torque and output, 3D finite element analysis (FEA) was performed by adjusting the input current. The results are shown in Table 4. When the performance of each case was considered, Case 4 exhibited the best performance under the same conditions.

Table 3. Spatial harmonics in the winding distributions of the considered cases.

Harmonic Order	Case 1	Case 2	Case 3	Case 4	Case 5
2	0.43	0	0	0	0
4	0.22	0	0	0	0
5	0.17	0.17	0.20	0.01	0.05
7	0.12	0.12	0.14	0.01	0.04
8	0.11	0	0	0	0
10	0.09	0	0	0	0
11	0.08	0.08	0.09	0.08	0.09
13	0.07	0.07	0.08	0.07	0.07

Table 4. 3D electromagnetic analysis for the considered cases.

Parameter	Case 1	Case 2	Case 3	Case 4	Case 5
Torque (Nm)	0.2865	0.2865	0.2865	0.2865	0.2865
Torque ripple (%)	15.66	3.97	4.03	1.32	1.12
Power (kW)	3	3	3	3	3
Rotor core loss (W)	4.37	3.92	3.86	4.09	4.06
Stator core loss (W)	48.71	43.48	43.06	51.72	52.77
PM loss (W)	499.23	114.63	103.99	6.07	11.70
Winding loss (W)	58.89	68.23	66.60	55.70	63.25
Efficiency (%)	83.07	92.87	93.24	96.23	95.79

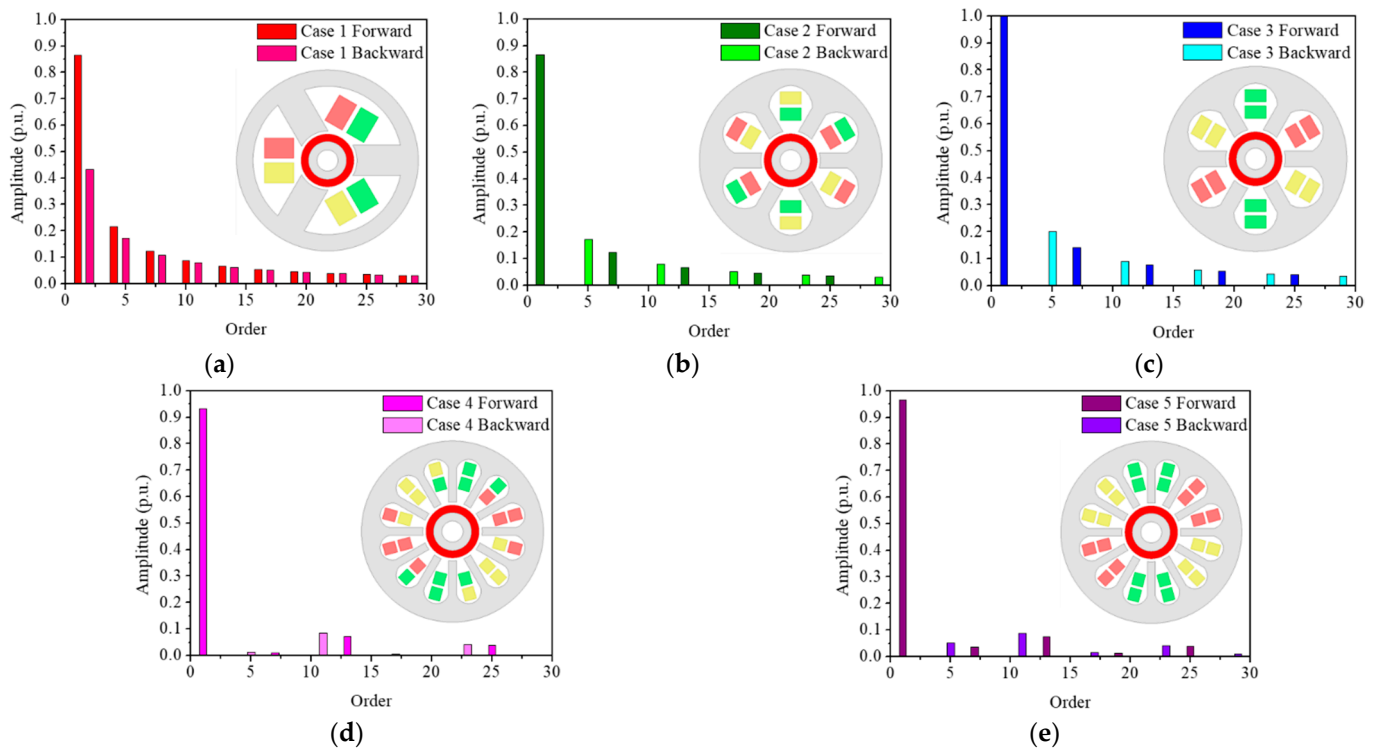


Figure 3. Results of the spatial harmonic analysis for the five cases considered according to pole/slot combination and winding configuration: (a) Case 1: 2P3S, concentrated; (b) Case 2: 2P6S, distributed (short); (c) Case 3: 2P6S, distributed (Full); (d) Case 4: 2P12S, distributed (short); and (e) Case 5: 2P12S, distributed (Full).

3. Analytical Model According to Eccentricity

The healthy condition of the motor is when the center of the rotor and that of the stator are coincident. This allows the radial electromagnetic forces to cancel out and the tangential ones to produce balanced torque with an identical air-gap. However, it is difficult to get perfect coincidence of the rotor and stator symmetrical axes due to manufacturing imperfections, issues during operation, or other reasons. Hence, the inherent level of static or dynamic eccentricity is typically within 10% of the air-gap. Such eccentricity results in bearing damage, unbalanced magnetic pull (UMP), and excessive noise and vibration. Consequently, it may cause the rotor poles to rub against the stator poles, resulting in gradual deterioration of the motor. The eccentricity consists of static eccentricity (SE), dynamic eccentricity (DE), and mixed eccentricity (ME), as shown Figure 4. SE in electrical motors occurs when the rotor symmetrical axis is concentric with the rotor rotational axis, but is dislocated with respect to the stator symmetrical axis. Hence, the position of the minimum radial air-gap length is fixed. This can be caused by stator core ovality, or incorrect positioning of the stator core or bearing at commissioning or following a repair. Its level usually does not change over time. DE occurs when the stator symmetrical axis is concentric with the rotor rotational axis, but is dislocated with respect to the rotor symmetrical axis. In this case, the position of the minimum radial air-gap rotates with the rotor. This can be caused by worn bearings, a bent shaft, asymmetric thermal expansion of the rotor, or by a high level of static eccentricity. The eccentricity in actual machinery often exhibits a combination of both types of eccentricity (defined as ME). These types of faults can be formulated following equations based on their geometric behavior [26–28].

$$\varepsilon = \left(\frac{r}{g} \right) \times 100 (\%) \quad (3)$$

$$r = \begin{cases} \left| \overrightarrow{O_s O_\omega} \right|, & \text{for SE} \\ \left| \overrightarrow{O_\omega O_r} \right|, & \text{for DE} \\ \left| \overrightarrow{O_s O_r} \right|, & \text{for ME} \end{cases} \quad (4)$$

where ε is the degree of eccentricity and g is the radial air gap length in the case of a uniform air gap. Here, O_r , O_s , and O_ω are the rotor, stator, and rotation symmetry centers, respectively. The three vectors in (4) are the static, dynamic, and mixed transfer vectors.

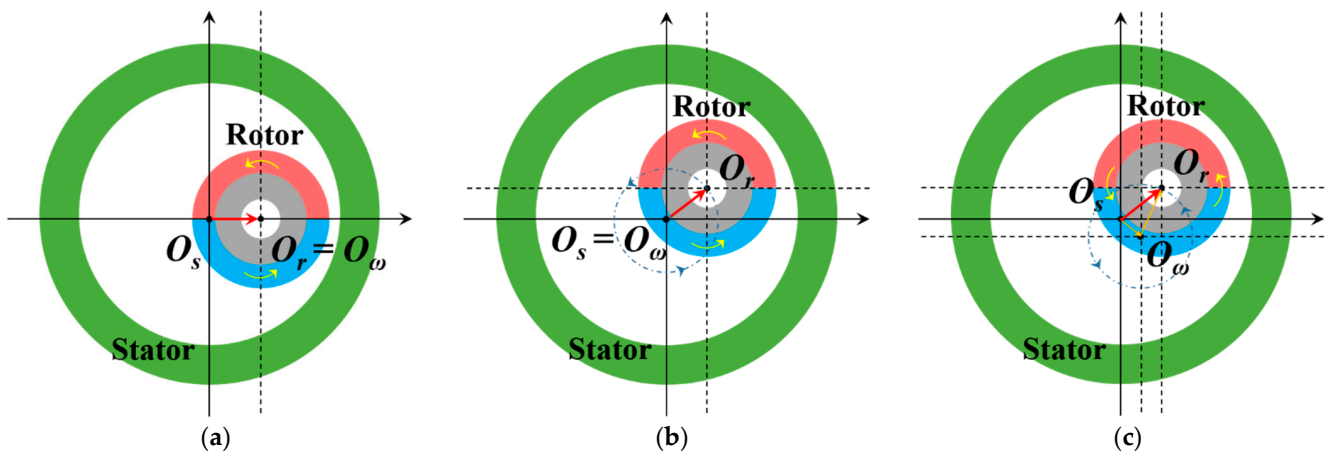


Figure 4. Positions of the stator, rotor, and rotation centers according to eccentricity: (a) Static eccentricity; (b) Dynamic eccentricity; (c) Mixed eccentricity.

4. Electrical Characteristics

When eccentricity occurs and the balance of the motor magnetic circuit is broken, the result is UMP. In other words, there is a force that pulls the rotor to one side as well as rotation torque, and this force is transmitted to the bearing, causing noise and vibration, and accelerating deterioration of the bearing. As mentioned in the previous section, for this paper, the electrical characteristics of the three eccentricities were analyzed in a healthy condition, and when the eccentricity was 25% and 50%. The waveform of the current supplied from a DC power source to the motor through an inverter was examined. That waveform supplies the current of the space vector pulse width modulation (SVPWM) waveform in which harmonic components are mixed in a sine wave. Therefore, in the two-dimensional (2D) electromagnetic field analysis with 12,459 elements, the SVPWM current waveform obtained through circuit simulation was applied as a current source to perform the analysis.

The electromagnetic force was calculated using the Maxwell stress tensor method as shown in (5) and (6) with the magnetic flux density in the radial direction and the tangential direction generated in the air-gap according to the amount of eccentricity. The electromagnetic force pressure at that time is shown in Figure 5 [29].

$$F_r = \frac{1}{2\mu_0} (B_r^2 - B_t^2) \quad (5)$$

$$F_t = \frac{1}{\mu_0} B_r B_t \quad (6)$$

When the static, dynamic, and mixed eccentricity was 25%, the difference in the electromagnetic force pressure between the healthy condition and eccentricity conditions was not much, but when mixed eccentricity occurred, the asymmetry of the pressure distribution in the radial direction increased. When the static, dynamic, and mixed eccen-

tricity was 50%, the difference in the electromagnetic force pressure between the healthy condition and eccentricity conditions was noticeable, and the asymmetry of the pressure distribution in the radial direction increased in the case of mixed eccentricity. Based on the results of the pressure distribution shown in Figure 5, it was predicted that the same eccentricity would have a large asymmetric force transmitted to the stator teeth in the order of mixed eccentricity, static eccentricity, and dynamic eccentricity, and would greatly affect the vibration.

In fact, when eccentricity occurs in an electric motor, not only one static eccentricity or dynamic eccentricity occurs; most cases involve mixed eccentricity with two at the same time. Hence, mixed eccentricity was applied to simulate an actual situation. This was also done to analyze clearly the effect of eccentricity because UMP is the largest. The changes in line inductance due to an irregular air-gap distance and UMP are shown in Figure 6 and Table 5. The change in line inductance between Phase A and Phase B was the largest.

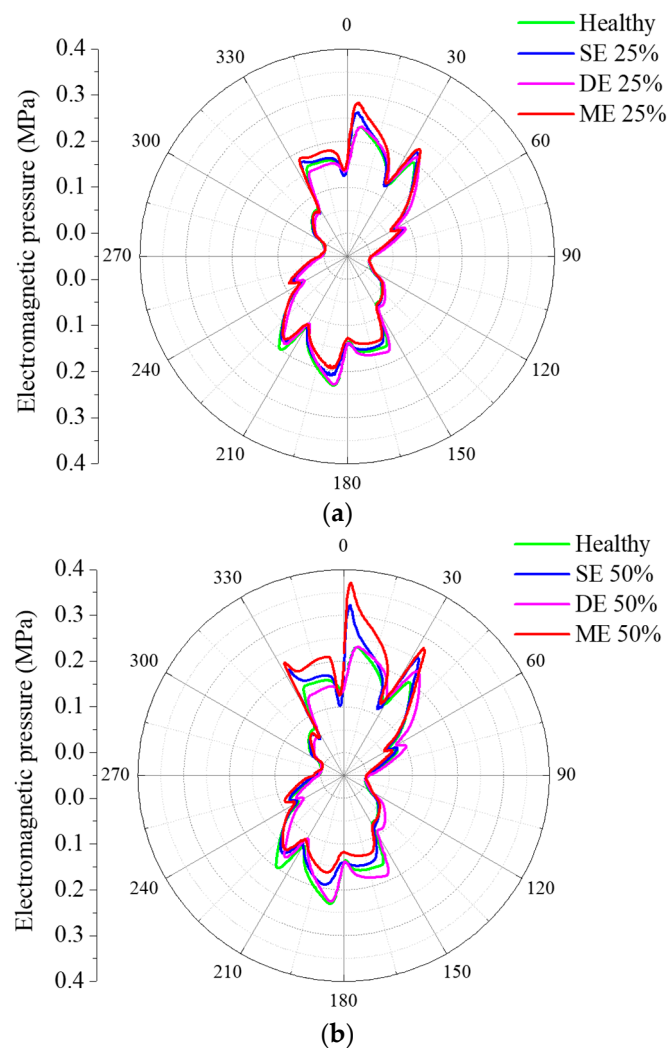


Figure 5. Electromagnetic pressure in the radial direction according to the amount of eccentricity: (a) Eccentricity 25% and (b) Eccentricity 50%.

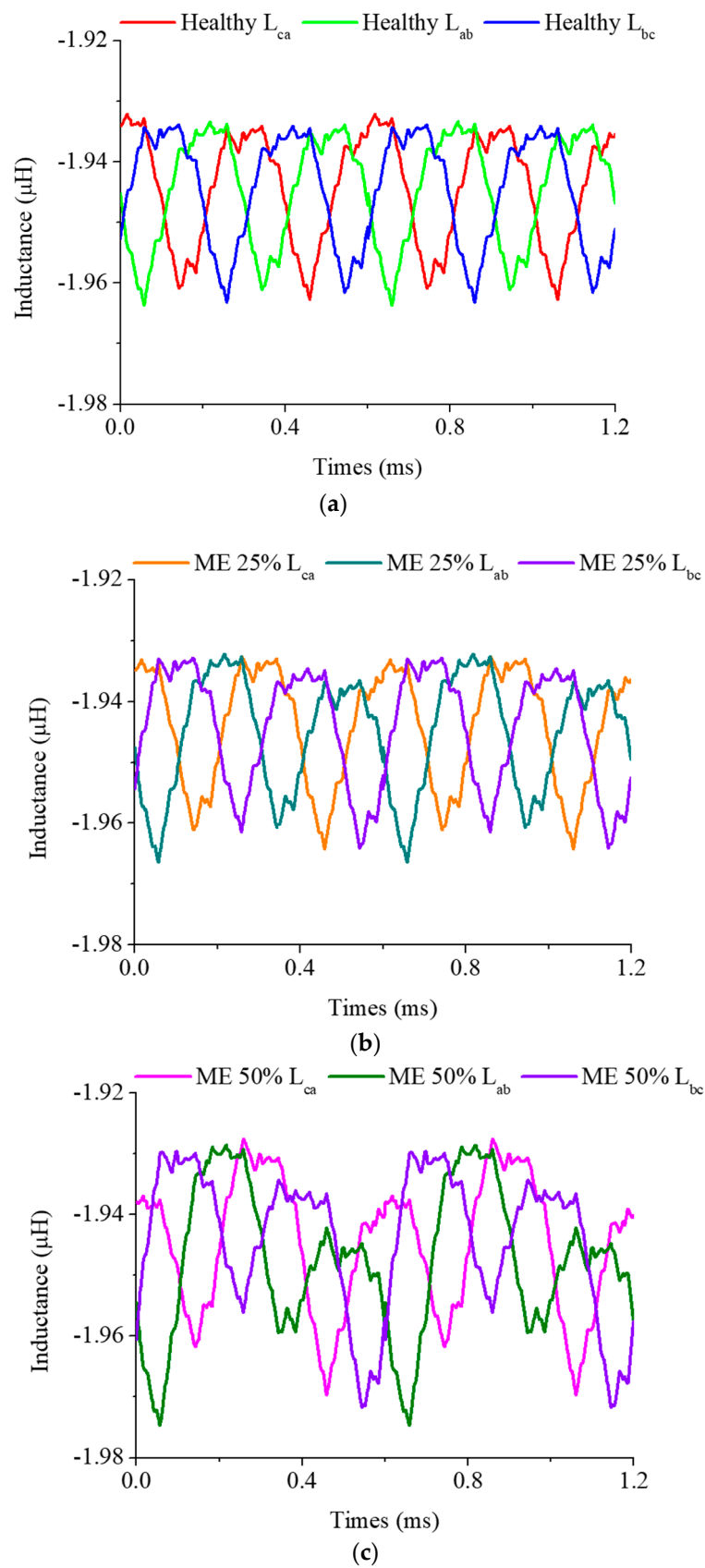
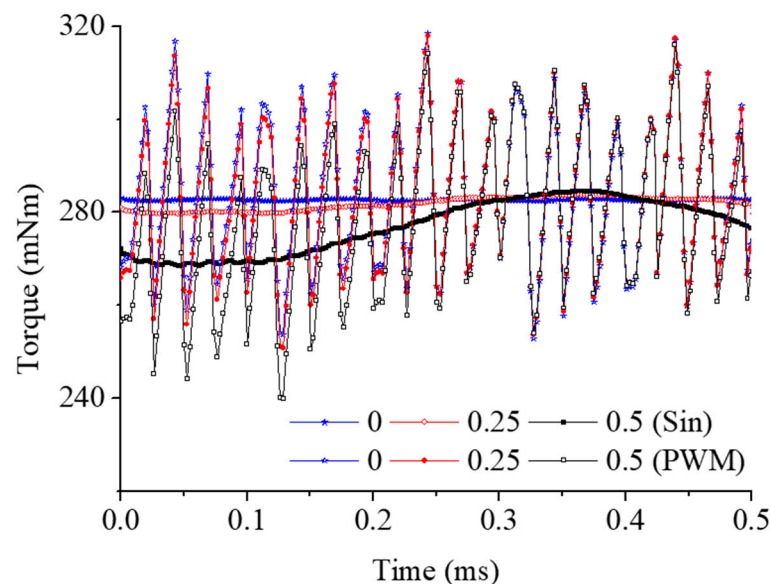


Figure 6. Line inductance according to the amount of mixed eccentricity: (a) Healthy condition, (b) Mixed eccentricity 25%, and (c) Mixed eccentricity 50%.

Table 5. Line-to-line inductance (absolute value) according to mixed eccentricity.

Mixed Eccentricity	L_{ca} (μH)	Error (%)	L_{ab} (μH)	Error (%)	L_{bc} (μH)	Error (%)
0%	1.9627	-	1.9637	-	1.9632	-
25%	1.9643	0.0815	1.9664	0.1375	1.9641	0.0458
50%	1.9697	0.3567	1.9746	0.5551	1.9718	0.4381

Figure 7 and Table 6 show average torque, torque ripple ratio, and maximum flux density according to current waveforms, and mixed eccentricity considering static and dynamic eccentricity. Comparing the ideal case where the current of a sine waveform is applied and the actual case where a PWM current waveform close to the sinusoidal wave is supplied, the average difference was 22.6% depending on the amount of eccentricity. In terms of the torque ripple ratio according to the amount of eccentricity in the same current waveform, the torque ripple ratio increased by 5.84% from 0.26% to 6.1% in the sine current waveform. On the other hand, for the PWM current waveform, the torque ripple ratio increased by 5.2% from 23.1% to 28.3%. The maximum flux density was the same according to the degree of eccentricity regardless of the current waveform.

**Figure 7.** Electromagnetic field analysis results according to eccentricity and current waveforms.**Table 6.** Comparison of torque, torque ripple, and maximum flux density according to eccentricity and current waveforms.

Mixed Eccentricity	Sine Waveform ($62A_{\text{rms}}$)			PWM Waveform ($64.7A_{\text{rms}}$)		
	Torque (mNm)	Ripple (%)	Max. Flux Density (T)	Torque (mNm)	Ripple (%)	Max. Flux Density (T)
0%	282	0.26	1.63	285	23.1	1.61
25%	281	1.24	1.65	284	24.0	1.65
50%	275	6.1	1.73	278	28.3	1.73

5. Mechanical Characteristics

Based on the results of electromagnetic analysis with eccentricity effect in the previous section, forced vibration analysis was performed as shown in Figure 8. The calculated electromagnetic forces (load) in the radial and tangential directions at the end of each stator tooth (with its harmonic components in the time domain) were converted into the frequency

domain using a fast Fourier transform (FFT). Then, the frequency components of the load were applied as the exciting force in a 3D model of motor and jig with 878,784 elements.

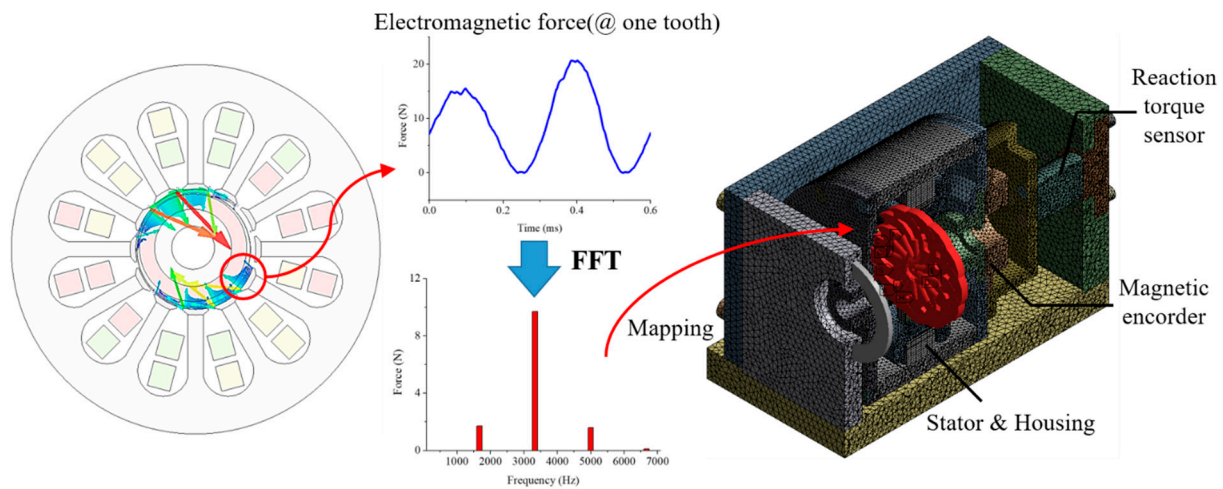


Figure 8. Concept of forced vibration (electromagnetic-structural one-way coupled) analysis.

Figure 9 shows the results of the vibration velocity in the Y-axis direction for the degree of mixed eccentricity. In the healthy condition, the vibration velocity was shown only at the pole passing frequency, which is the excitation frequency caused by the typical electromagnetic force generated by an electric motor. The vibration mode can be predicted using the greatest common divisor (GCD) of the number of poles and the number of slots. Because the GCD of this motor is 2, it is expected that an elliptical vibration mode was observed. In the analysis results, an elliptical vibration mode was observed at the pole passing frequency (3333.33 Hz). As the degree of mixed eccentricity increased, the vibration velocity was also observed at a frequency that was half of the pole passing frequency (1666.67 Hz), and the frequency generated by the eccentricity became resonant with the natural frequency of the model, resulting in a large peak. It was confirmed that the eccentricity effect creates other frequencies aside from the pole passing frequency. Thus, the presence or absence of eccentricity can be evaluated by measuring the vibration later.

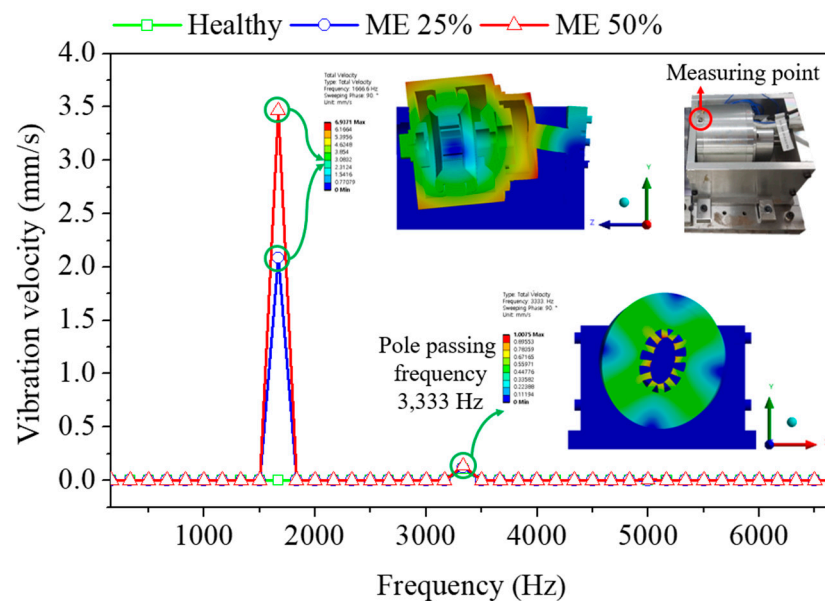


Figure 9. Vibration velocity of Y-axis direction considering mixed eccentricity and measuring point.

6. Conclusions

In this paper, the electrical and mechanical characteristics of a high-speed motor were analyzed according to various eccentricities using ANSYS software. Before analyzing the effect of eccentricity, a 2P12S motor with distributed windings (short pitch) was selected through comparisons of winding factor, spatial harmonics analysis, and electromagnetic field analysis for a variety of models according to the number of poles and slots and winding method. Based on the selected model, electromagnetic field analysis, and forced vibration analysis were performed to determine their static, dynamic, and mixed eccentricity. When the degree of eccentricity increased to 50%, the imbalance of the line inductance became more severe and the discrepancy between the healthy condition and ME 50% was 0.55%. Moreover, it was confirmed that other vibration frequencies (in addition to the pole passing frequency or excitation frequency) were generated at half the pole passing frequency (1666.67 Hz) in the forced vibration analysis. Eccentricity can be predicted by confirming the change in the magnitude of the winding inductance and the imbalance of the line-to-line waveform proposed in this paper. In the future, we plan to compare the prediction of eccentricity with the analysis result due to the imbalance of the waveform between lines of inductance when driving the motor. We also plan to measure the actual vibration and compare it with the results from forced vibration analysis.

Author Contributions: Conceptualization, T.-W.L. and D.-K.H.; software, T.-W.L.; validation, T.-W.L. and D.-K.H.; investigation, T.-W.L.; writing—original draft preparation, T.-W.L.; writing—review and editing, T.-W.L.; visualization, T.-W.L.; supervision, D.-K.H.; project administration, D.-K.H. Both authors have read and agreed to the published version of the manuscript.

Funding: This work was supported by the UST Young Scientist Research Program 2020 through the University of Science and Technology, Korea (No. 2020YS30) and was supported by the Ministry of Trade, Industry and Energy (MOTIE, Korea) under the Industrial Technology Innovation Program [No.10062541, “Development of electric compressor to improve low end torque performance and transient performance of 1.6 L grade small diesel engine”].

Institutional Review Board Statement: Not applicable.

Informed Consent Statement: Not applicable.

Data Availability Statement: Some or all of the data and the models generated or used during the study, are available in a repository or online.

Acknowledgments: This project was conducted jointly with KERI, Keyyang Precision, Hanyang University, and Kookmin University.

Conflicts of Interest: The authors declare no conflict of interest.

Abbreviations

BLAC	Brushless alternating current
BLDC	Brushless direct current
CO ₂	Carbon dioxide
DE	Dynamic eccentricity
EAT	Electrically assisted turbocharger
EC	Electric compressor
EFIS	Electric forced induction systems
EST	Electrically split turbocharger
ETC	Electric turbocharger
FEA	Finite element analysis
FFT	Fast Fourier transform
FIS	Forced induction systems
GCD	Greatest common divisor
IM	Induction motors
ME	Mixed eccentricity
MMF	Magnetomotive force

PM	Permanent magnet
PMSM	Permanent magnet synchronous motors
PWM	Pulse width modulation
SE	Static eccentricity
SPMSM	Surface mounted permanent magnet synchronous motors
SRM	Switched reluctance motors
SVPWM	Space vector pulse width modulation
TEDC	Turbocharger with an additional electrically driven compressor
UMP	Unbalanced magnetic pull
VGT	Variable geometry turbocharger

References

- Lee, W.; Schubert, E.; Li, Y.; Li, S.; Bobba, D.; Sarlioglu, B. Overview of Electric Turbocharger and Supercharger for Downsized Internal Combustion Engines. *IEEE Trans. Transp. Electrification*. **2017**, *3*, 36–47. [\[CrossRef\]](#)
- Hiereth, H.; Prenninger, P. *Charging the Internal Combustion Engine*, 1st ed.; Springer: Wien, Austria, 2003; pp. 1–4.
- Yamashita, Y.; Ibaraki, S.; Sumida, O.; Ebisu, K.I.; An, I.L.; Ogita, I. Development of electric supercharger to facilitate the downsizing of automobile engines. *Mitsubishi Heavy Ind. Tech. Rev.* **2010**, *47*, 7–12.
- Gödeke, H.; Prevedel, K. Hybrid turbocharger with innovative electric motor. *MTZ Worldw.* **2014**, *75*, 26–31. [\[CrossRef\]](#)
- Ibaraki, S.; Yamashita, Y.; Sumida, K.; Ogita, H.; Jinnai, Y. Development of the ‘hybrid turbo’, an electrically assisted turbocharger. *Mitsubishi Heavy Ind. Tech. Rev.* **2006**, *43*, 1–5.
- Woollenweber, W.E.; Halimi, E.M. Motor-Generator Assisted Turbocharging Systems for Use with Internal Combustion Engines and Control Method Therefor. U.S. Patent US5906098A, 25 May 1999.
- Arnold, S.; Balis, C.; Barthelet, P.; Poix, E.; Samad, T.; Hampson, G.; Shahed, S.M. Garrett electric boosting systems (EBS) program. *Honeywell Turbo Technol.* **2005**. Available online: <https://www.osti.gov/servlets/purl/910121> (accessed on 1 June 2021).
- Hofbauer, P. Method of Controlling an Electrically Assisted Turbocharger. U.S. Patent US20110022289A1, 27 January 2011.
- Shimizu, M. Turbocharger with Electric Motor. U.S. Patent US8882478B2, 11 November 2014.
- Gill, N. Driving clean technology. In Proceedings of the Cleantech Forum Europe 2012, Munich, Germany, 16–18 April 2012.
- Breitbach, H.; Metz, D.; Weiske, S.; Spinner, G. *Application and Design of the eBooster from BorgWarner*; BorgWarner Turbo System GmbH: Auburn Hills, MI, USA, 2015.
- Biwersi, S.; Tavernier, S.; Equoy, S. Electric compressor with high-speed brushless DC motor. *MTZ Worldw.* **2012**, *73*, 50–53. [\[CrossRef\]](#)
- Menegazzi, P.; Wu, Y.; Thomas, V. Design of an electric supercharger for downsized engines. *MTZ Worldw.* **2013**, *74*, 36–41. [\[CrossRef\]](#)
- Noguchi, T.; Kano, M. Development of 150,000 r/min, 1.5 kW Permanent-Magnet Motor for Automotive Supercharger. In Proceedings of the 2007 PEDS, Bangkok, Thailand, 27–30 November 2007; pp. 183–188.
- Heidrich, T.; Ludwig, F.; Moeckel, A. Investigation of a high-speed drive for turbo-machines. In Proceedings of the Innovative Small Drives and Micro-Motor Systems, 11th GMM/ETG-Symposium, Saarbruecken, Germany, 27–28 September 2017; pp. 1–5.
- Lim, M.-S.; Kim, J.-M.; Hwang, Y.S.; Hong, J.-P. Design of an Ultra-High-Speed Permanent-Magnet Motor for an Electric Turbocharger Considering Speed Response Characteristics. *IEEE/ASME Trans. Mechatron.* **2017**, *22*, 774–784. [\[CrossRef\]](#)
- Hong, D.K.; Lee, T.W.; Jeong, Y.H. Design and Experimental Validation of a High-Speed Electric Turbocharger Motor Considering Variation of the L/D Ratio. *IEEE Trans. Magn.* **2018**, *54*, 1–4.
- Lee, W.; Kim, J.H.; Choi, W.; Sarlioglu, B. Torque Ripple Minimization Control Technique of High-Speed Single-Phase Brushless DC Motor for Electric Turbocharger. *IEEE Trans. Veh. Technol.* **2018**, *67*, 10357–10365. [\[CrossRef\]](#)
- Zhao, D.; Stobart, R.; Mason, B. Real-Time Energy Management of the Electric Turbocharger Based on Explicit Model Predictive Control. *IEEE Trans. Ind. Electron.* **2020**, *67*, 3126–3137. [\[CrossRef\]](#)
- Tran, H.H.; Richard, B.; Gray, K.; Hall, J.M. Developing a performance specification for an electric supercharger to satisfy a range of downsized gasoline engine applications. In Proceedings of the SAE 2016 World Congress & Exhibition, Detroit, MI, USA, 12–14 April 2016.
- Baek, S.; Woo, S.; Kim, Y.; Lee, K. Prediction of turbocharged diesel engine performance equipped with an electric supercharger using 1D simulation. *Energy* **2019**, *185*, 213–228. [\[CrossRef\]](#)
- Lee, T.W.; Baek, S.J.; Lee, K.H. Simulation and Motor Test Considering Engine Experiment Validation of Electric Turbocharger for 1.6L Diesel Engine. *IEEE Trans. Transp. Electrification*. under review.
- Hofmann, M.; Eckardt, B.; Heckel, T. Inverter technology for high-speed drives like electric turbochargers. In Proceedings of the IKMT 2015, 10. ETG/GMM-Symposium Innovative small Drives and Micro-Motor Systems, Cologne, Germany, 14–15 September 2015; pp. 1–6.
- Merdzan, M.; Paulides, J.J.H.; Lomonova, E.A. Comparative analysis of rotor losses in high-speed permanent magnet machines with different winding configurations considering the influence of the inverter PWM. In Proceedings of the 2015 Tenth International Conference on EVER, Monte Carlo, Monaco, 31 March–2 April 2015; pp. 1–8.

25. Imamura, R.; Lorenz, R.D. Lorenz. Stator Winding MMF Analysis for Variable Flux and Variable Magnetization Pattern PMSMs. *IEEE Trans. Ind. Appl.* **2020**, *56*, 2644–2653. [[CrossRef](#)]
26. Karami, M.; Mariun, N.; Rezazadeh Mehrjou, M.; Ab Kadir, M.Z.A.; Misron, N.; Mohd Radzi, M.A. Static eccentricity fault recognition in three-phase line start permanent magnet synchronous motor using finite element method. *Math. Probl. Eng.* **2014**, *2014*, 1–12. [[CrossRef](#)]
27. Torkaman, H.; Afjei, E.; Yadegari, P. Static, Dynamic, and Mixed Eccentricity Faults Diagnosis in Switched Reluctance Motors Using Transient Finite Element Method and Experiments. *IEEE Trans. Magn.* **2012**, *48*, 2254–2264. [[CrossRef](#)]
28. Hong, J.; Bin Lee, S.; Kral, C.; Haumer, A. Detection of Airgap Eccentricity for Permanent Magnet Synchronous Motors Based on the d-Axis Inductance. *IEEE Trans. Power Electron.* **2012**, *27*, 2605–2612. [[CrossRef](#)]
29. He, G.; Huang, Z.; Qin, R.; Chen, D. Numerical Prediction of Electromagnetic Vibration and Noise of Permanent-Magnet Direct Current Commutator Motors with Rotor Eccentricities and Glue Effects. *IEEE Trans. Magn.* **2012**, *48*, 1924–1931. [[CrossRef](#)]